J|A|C|S
ARTICLES

Published on Web 04/29/2009

Tunable Ferromagnetic Spin Ordering in Boron Nitride Nanotubes with Topological Fluorine Adsorption

Zhuhua Zhang and Wanlin Guo*

Institute of Nano Science, Nanjing University of Aeronautics and Astronautics, No. 29 of Yudao Street, Nanjing 210016, People's Republic of China

Received March 2, 2009; E-mail: wlguo@nuaa.edu.cn

Abstract: We find through first-principles calculations that fluorine atoms topologically adsorbed on boron nitride nanotubes induce long-ranged ferromagnetic spin ordering along the tube, offering strong spin polarization around the Fermi level. The spin polarization and magnetic moment increase significantly with decreasing tube radius, even giving rise to half-metal when the tube diameter is reduced to 3.3 Å, while in a flat boron nitride sheet with the same topological fluorine arrangement the magnetic moment nearly disappears. This radius-dependent behavior is then developed into a local curvature modulation procedure to efficiently enhance or quench the ferromagnetic ordering, which enables the F-BNNTs to function as piezomagnetic nanotubes. These findings suggest a new route to facilitate the design of tunable spin devices.

Introduction

Light element magnets hold great promise to overcome the limitations of technologies relying on current magnetic materials based on d and f elements as they involve only sp elements. This topic has captured a rapid surge of interest since magnetism was experimentally observed in polymeric fullerenes[1] and graphite.[2,3] Despite great theoretical efforts, the predicted magnetism is mostly induced by localized electron states in a variety of zero-,[4−6] two-dimensional (2D),[7−11] and bulk[12,13] metal-free materials. Nevertheless, for use in nanoelectronics, one-dimensional (1D) nanoscale magnets with ferromagnetic (FM) spin ordering are more desirable. This requires FM coupling among the polarized electron spins in nanostructures. Such magnetic ordering has been observed in zigzag edges of graphite ribbons[14−16] as well as carbon nanotubes (CNTs) with topological line defects.[17,18] Yet the number of polarized electron spins in these systems is relatively small and nearly independent of the ribbon width or tube diameter, and therefore is inconvenient to control. In complete analogy to CNTs, boron nitride nanotubes[19−21] (BNNTs) have been attracting much interest due to their unique properties, especially their high thermal stability and chemical inertness. It has been shown that the electric conductance of the BNNTs can be significantly enhanced by surface fluorination,[22,23] and their physical and chemical natures exhibit remarkable radius dependence.[24] What is more, spontaneous magnetization can be induced in the BNNTs by fluorination[25] or dopant substitutions.[26−28] Thus, it becomes much intriguing if the FM spin ordering can be obtained in the potential BNNTs. Moreover, modulating spin transport in a well-controlled manner is central to actual applications. Alternative

(1) Makarova, T. L.; Sundqvist, B.; Hohne, R.; Esqulnazl, P.; Kopelevich, K.; Scharff, P.; Davydov, V. A.; Kahsevarova, L. A.; Rakhmanina, A. V. *Nature* **2001**, *413*, 716–718.
(2) Shibayama, Y.; Sato, H.; Enoki, T.; Endo, M. *Phys. Rev. Lett.* **2000**, *84*, 1744–1747.
(3) Esquinazi, P.; Spemann, D.; Hohne, R.; Setzer, A.; Han, K. H.; Butz, T. *Phys. Rev. Lett.* **2003**, *91*, 227201.
(4) Park, N.; Yoon, M.; Berber, S.; Ihm, J.; Osawa, E.; Tománek, D. *Phys. Rev. Lett.* **2003**, *91*, 237204.
(5) Fernandez-Rossier, J.; Palacios, J. J. *Phys. Rev. Lett.* **2007**, *99*, 177204.
(6) Hao, S.; Zhou, G.; Duan, W.; Wu, J.; Gu, B. *J. Am. Chem. Soc.* **2006**, *128*, 8453–8458.
(7) Vozmediano, M. A. H.; López-Sancho, M. P.; Stauber, T.; Guinea, F. *Phys. Rev. B* **2005**, *72*, 155121.
(8) Yazyev, O. V.; Helm, L. *Phys. Rev. B* **2007**, *75*, 125408.
(9) Lehtinen, P. O.; Foster, A. S.; Ayuela, A.; Krasheninnikov, A.; Nordlund, K.; Nieminen, R. M. *Phys. Rev. Lett.* **2003**, *91*, 017202.
(10) Andriotis, A. N.; Menon, M.; Sheetz, R. M.; Chernozatonskii, L. *Phys. Rev. Lett.* **2003**, *90*, 026801.
(11) Lehtinen, P. O.; Foster, A. S.; Ma, Y.; Krasheninnikov, A. V.; Nieminen, R. M. *Phys. Rev. Lett.* **2004**, *93*, 187202.
(12) Zhang, Y.; Talapatra, S.; Kar, S.; Vajtai, R.; Nayak, S. K.; Ajayan, P. M. *Phys. Rev. Lett.* **2007**, *99*, 107201.
(13) Lee, K. W.; Lee, C. E. *Phys. Rev. Lett.* **2006**, *97*, 137206.
(14) Nakada, K.; Fujita, M.; Dresselhaus, G.; Dresselhaus, M. S. *Phys. Rev. B* **1996**, *54*, 17954–17961.
(15) Kusakabe, K.; Maruyama, M. *Phys. Rev. B* **2003**, *67*, 092406.
(16) Lee, H.; Son, Y.; Park, N.; Han, S.; Yu, J. *Phys. Rev. B* **2005**, *72*, 174431.
(17) Okada, S.; Nakada, K.; Kuwabara, K.; Daigoku, K.; Kawai, T. *Phys. Rev. B* **2006**, *74*, 121412.
(18) Alexandre, S. S.; Mazzoni, M. S. C.; Chacham, H. *Phys. Rev. Lett.* **2008**, *100*, 146801.
(19) Rubio, A.; Corkill, J. L.; Cohen, M. L. *Phys. Rev. B* **1994**, *49*, 5081–5084.
(20) Chopra, N.; Luyken, J.; Cherry, K.; Crespi, V. H.; Cohen, M. L.; Louie, S. G.; Zettl, A. *Science* **1995**, *269*, 966–967.
(21) Zhang, Z. H.; Guo, W. L.; Tai, G. *Appl. Phys. Lett.* **2007**, *90*, 133103.
(22) Tang, C.; Bando, Y.; Huang, Y.; Yue, S.; Gu, C.; Xu, F.; Golberg, D. *J. Am. Chem. Soc.* **2005**, *127*, 6552–6553.
(23) Xiang, H. J.; Yang, J.; Hou, J. G.; Zhu, Q. *Appl. Phys. Lett.* **2005**, *87*, 243113.
(24) Xiang, H. J.; Yang, J.; Hou, J. G.; Zhu, Q. *Phys. Rev. B* **2003**, *68*, 035427.
(25) Li, F.; Zhu, Z.; Yao, X.; Lu, G. *Appl. Phys. Lett.* **2008**, *92*, 102515.
(26) Li, J.; Zhou, G.; Chen, Y.; Gu, B.; Duan, W. *J. Am. Chem. Soc.* **2009**, *131*, 1796–1801.
(27) Wu, R. Q.; Liu, L.; Peng, G. W.; Feng, Y. P. *Appl. Phys. Lett.* **2005**, *86*, 122510.
(28) Guo, C. S.; Fan, W. J.; Zhang, R. Q. *Appl. Phys. Lett.* **2006**, *89*, 123103.
(29) Abolfath, R. M.; Petukhov, A. G.; Zutic, I. *Phys. Rev. Lett.* **2008**, *101*, 207202.
(30) Son, Y.; Cohen, M. L.; Louie, S. G. *Nano Lett.* **2007**, *7*, 3518–3522.

10.1021/ja901586k CCC: $40.75

approaches of magnetic modulation through external force[29] or fields[30,31] and doping[32,33] have been proposed in various nanostructures, but in light-element magnets the acquisition of controllable spin ordering remains an important challenge.

Here, we report comprehensive first-principles studies on the electronic and magnetic properties of topologically fluorinated BNNTs (F-BNNTs). It is shown that the F-BNNTs exhibit surprising long-ranged magnetic ordering that polarized electron spins are localized around adsorption sites and ferromagnetically aligned along the tube axis, offering strong spin polarization around the Fermi level. The spin polarization and magnetic moment increase rapidly with decreasing tube diameter, even translating to half-metal when the tube size is reduced to (4,0). Motivated by these results, we propose and demonstrate a nanomechanical modulation of tube curvature by radial deformation to sensitively enhance or quench the spin polarization of large F-BNNTs. Our work offers a new avenue for controllable and tunable spintronic devices.

Theory and Methods

The calculations in this work were performed within the framework of density functional theory as implemented in VASP code.[34−36] Ultrasoft pseudopotentials[37] for the core region and the local spin density approximation (LSDA) for the exchange-correlation potential were used. A kinetic energy cutoff of 530 eV was used in the plane-wave expansion. The supercell consists of an F atom and a primitive tube cell, thus forming an F chain along the BNNT within periodic boundary condition. The distances between two adjacent nanotubes were held at at least 11 Å to eliminate the interaction between them. The Brillouin-zone integration was sampled by up to 20 special k points for geometry relaxation and total 50 k points for electronic structure calculations. The changes in magnetic moment and total energy are less than 10^{-4} μ_B (μ_B is the Bohr magneton) and 1 meV, respectively, with further increasing number of k points. The structures were fully relaxed using the conjugate gradient method until the force on each atom was less than 0.01 eV/Å. We verified that the LSDA did not give an artificial spin polarization. We have performed test calculations using generalized gradient approximation, and hybrid B3LYP,[38] showing the same qualitative results. The minimum energy path (MEP) was mapped out using the climbing image nudged elastic band method.[39,40] All molecular dynamics (MD) simulations were carried out in the canonical ensemble by means of a Nosé thermostat to control temperature, and Newton's equations of motion were integrated using the Verlet algorithm.

Results and Discussion

Because of the chirality preference of zigzag orientation during the growth of BNNTs,[41] here we focus on zigzag BNNTs. For F chemisorption on BNNTs, the F atoms adsorb directly on top of the B atoms, which is energetically the most favorable.[23] The structure of the optimized (6,0) F-BNNT is shown in Figure 1a, together with the corresponding spin density, or charge density for spin up minus spin down. It is exciting that the F-BNNT exhibits magnetic ordering: The polarized electron spins are aligned along the tube axis, and the distribution of the spins remarkably decreases with increasing distance from the adsorption site. The magnetic moment per supercell is calculated to be about 0.67 μ_B, mainly contributed by the N atoms 1 (0.27 μ_B), 2 (0.063 μ_B), and 3 (0.063 μ_B) bonding to the fluorinated B atom as denoted in Figure 1a. The F atom and all of the B atoms have little contribution to the moment (about 0.02 and 0.04 μ_B, respectively). It is known that F atom possesses strong electron affinity, which enables it loot electrons from the BNNT. Bader analysis[42] shows that the lost electrons in the (6,0) BNNT are dominantly from the N atoms, which is also supported by the analysis of charge redistribution driven by the adsorption of fluorine (not shown). The magnetic moment contributed by each N atom is actually proportional to the number of holes on it.

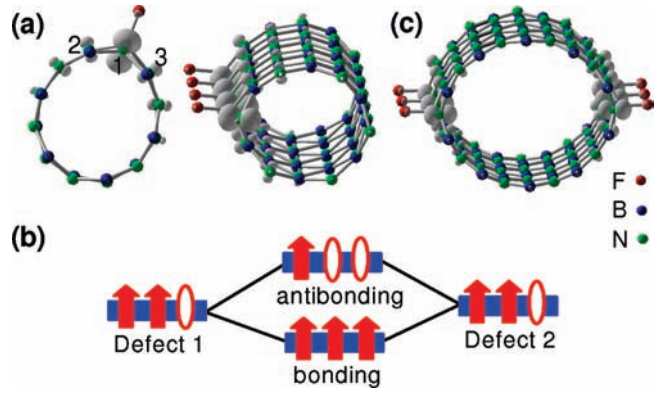

Figure 1. Iso-surface plots (0.15 e/Å^3) of magnetization density of the F-BNNTs. (a) The axial and side views of the (6,0) F-BNNT. (b) Schematic illustration of the exchange coupling mechanism for ferromagnetism in the F-BNNTs. The red arrow and ellipse represent the electron in a spin direction and the hole, respectively. (c) The (10,0) F-BNNT with two diametrically opposed F chains, together with the iso-surface plot (0.15 e/Å^3) of spin density.

The existence of magnetic moment does not necessarily result in FM spin ordering. It thus is necessary to study the magnetic coupling between the adsorption-induced moments. We doubled the size of the supercell, and each supercell now contains two F atoms. Depending on the initial conditions of self-consistent calculations, two stable magnetic structures are obtained: one is FM and the other antiferromagnetic (AFM). Total energy calculations show that the energy difference, ΔE, between the AFM and FM phases is $E^{AFM} - E^{FM} = 16$ meV. To drive the strength of the exchange coupling, we employ a 1D Heisenberg model, $H = -J\Sigma_i\sigma_i\sigma_{i+1}$, where J is the exchange coupling parameter, and σ_i is the net spin induced by the ith chemisorption. On the basis of this model, ΔE can also be deduced as $E^{AFM} - E^{FM} = 2J|\sigma_i|^2$. Comparing this result with ΔE from ab initio calculations, a positive exchange coupling $J = 32$ meV is yielded in this system, indicating an appreciable magnetic coupling. The exchange coupling J can be increased by radial

(31) Liao, Z. M.; Li, Y. D.; Xu, J.; Zhang, J. M.; Xia, K.; Yu, D. P. *Nano Lett.* **2006**, *6*, 1087–1091.
(32) Dev, P.; Xue, Y.; Zhang, P. *Phys. Rev. Lett.* **2008**, *100*, 117204.
(33) Roddaro, S.; Fuhrer, A.; Brusheim, P.; Fasth, C.; Xu, H. Q.; Samuelson, L.; Xiang, J.; Lieber, C. M. *Phys. Rev. Lett.* **2008**, *101*, 186802.
(34) Kresse, G.; Hafner, J. *Phys. Rev. B* **1993**, *47*, 558–561.
(35) Kresse, G.; Hafner, J. *Phys. Rev. B* **1994**, *49*, 14251–14269.
(36) Kresse, G.; Furthmuller, J. *Phys. Rev. B* **1996**, *54*, 11169–11186.
(37) Vanderbilt, D. *Phys. Rev. B* **1990**, *41*, 7892–7895.
(38) The hybrid B3LYP calculations are implemented in PCGAMESS with the 6-31G* basis set.
(39) Mills, G.; Jonsson, H.; Schenter, G. K. *Surf. Sci.* **1995**, *324*, 305–337.
(40) Henkelman, G.; Uberuaga, B. P.; Jonsson, H. *J. Chem. Phys.* **2000**, *113*, 9901–9904.
(41) Terauchi, M.; Tanaka, M.; Suzuki, K.; Ogino, A.; Kimurab, K. *Chem. Phys. Lett.* **2000**, *324*, 359–364.
(42) Henkelman, G.; Arnaldsson, A.; Jónsson, H. *Comput. Mater. Sci.* **2006**, *36*, 354–360.

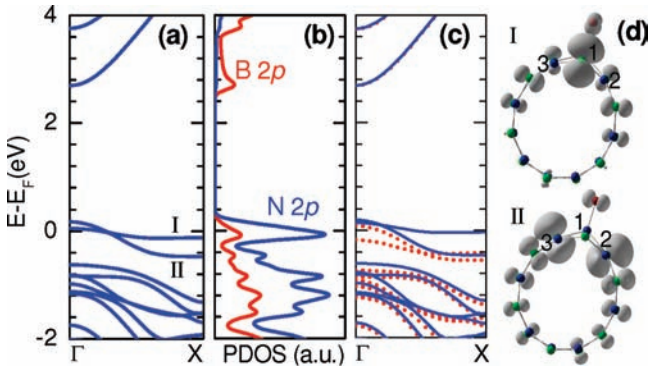

Figure 2. Band structures of the (6,0) F-BNNT. (a) Spin-unresolved band structure. (b) Partial density of state (PDOS) of the boron and nitrogen 2p states. (c) Spin-resolved band structure (majority spin, red dash line; minority spin, black solid line). The Fermi level is set to zero. (d) Iso-surface plots (0.045 e/Å^3) for charge density of bands I and II as denoted in (a).

deformation. For example, under a radial strain of 0.5, J is enhanced to 68 meV, making the F-BNNTs even attractive for room-temperature ferromagnetism. This mechanical modulation effect will be particularly discussed later. The FM coupling results from the extended defect states induced by F adsorption that are over half-filling, evidencing the existence of partially occupied levels. According to the level coupling model proposed by Mahadevan et al.,[43] virtual electron hopping is only allowed for the FM alignment due to the energy gain from degenerate interacting levels as illustrated in Figure 1b.

The origin of magnetism in the F-BNNT is related to its electronic structures. Figure 2a shows the spin-unpolarized band structures of the (6,0) F-BNNT, where two partial-filled bands I and II (called defect bands thereafter) appear at the Fermi level and act as shallow acceptors, in line with previous results.[23] Both of the defect bands are much flattened, indicating that the corresponding electron states are heavily localized. The localization of the two defect states can also be visualized by plotting their charge distribution in real space as shown in Figure 2d. It is evident that the two defect states are strongly localized on the three N atoms surrounding the adsorption site. Especially, band I shows its charge density highly concentrated on the N atom 1, but band I possesses a small dispersion of 0.17 eV, arising from the periodic potential along the tube axis induced by topological F adsorption. In contrast, band II with a dispersion of 0.65 eV shows its dominant density on the N atoms 2 and 3, and weak $\pi-\pi$ interaction between them makes band II slightly higher in energy than band I near the Γ point. Both of the bands are mainly contributed by the nitrogen 2p states that exhibit a sharp peak at the Fermi level (Figure 2b). According to Hund's rule, partial filling of the localized bands drives spontaneous spin polarization, resulting in an exchange splitting of 0.32 and 0.11 eV for bands I and II (Figure 2c), respectively. Following the exchange splitting, the total energy of the system is lowered by 21.5 meV from that of the nonmagnetic state. Meanwhile, strong spin polarization is found in the vicinity of the Fermi level as shown in Figure 3a. The spin polarization,[44] $P = (N_\downarrow(E_F) - N_\uparrow(E_F))/(N_\downarrow(E_F) + N_\uparrow(E_F))$, where $N_\downarrow(E_F)$ and $N_\uparrow(E_F)$ represent the DOS corresponding to the minority and majority spins at the Fermi level, respectively, is calculated to be 63%, which is even close to those of cobalt/CNT hybrid structures.[45]

Some factors should be clarified to discuss the spin ordering in the F-BNNT. The first factor is the dimensionality effect. We first uncurl the (6,0) F-BNNT into a fluorinated BN nanoribbon, with the dangling bonds on both edges terminated by hydrogen. Next, the LSDA calculations obtain a moment of 0.51 μ_B per supercell in the fluorinated ribbon, smaller than that of the (6,0) F-BNNT. However, the BN sheet with the same topological F arrangement is nearly nonmagnetic. In the case of flat BN sheet, the corresponding band I has a large dispersion of 0.72 eV and becomes almost occupied, mainly due to that the extended character of the defect states results in another Fermi surface near the 2D Brillouin-zone boundary. So the dimensionality effect, the lateral confinement, is crucial for the occurrence of magnetic ordering in the F-BNNTs. Next, the effect of F diffusion is studied by carefully examining the magnetism of the cases with F atom adsorbed on other possible sites. We consider two additional adsorption sites: on top of the N atom and on the B−N bond. For the two configurations, the calculated magnetic moments per supercell are about 0.98 μ_B and 1.0 μ_B, respectively, but it is extremely unlikely for these configurations because of the high diffusion barriers for F atom from the top of the B atom to these adsorption sites. In fact, the F atoms spontaneously returned to the B sites when the two configurations were fully relaxed without any constraint. Another point is that charge injection into the F-BNNT should drastically affect its magnetism, because the moment value is mainly determined by the hole population in BNNTs. When an electron is doped in the supercell,[46] the spin in the (6,0) F-BNNT is quenched. The injected electron compensates the holes in the supercell and just makes bands I and II fully occupied. The occupied states, although localized, cannot cause exchange splitting. Nevertheless, when a hole is introduced in the same system, the magnetic moment per supercell is enhanced up to 0.9 μ_B, higher than the undoped level. The injected hole mainly distributes on the N atoms 1, 2, and 3 due to the higher levels of the defect states than of all other valence states. For example, the hole on the N atom 1 increases to 0.47|e|, triggering a large moment of 0.41 μ_B. So the enhancement of moment is mainly from the three N atoms (0.17 μ_B in total) and little from the B atoms (0.02 μ_B in total). These results suggest an experimentally viable way for tailoring magnetism in the F-BNNTs. Similar control of magnetism has been demonstrated in wide-gap III nitrides with cation-vacancy.[32]

We last examine the magnetism in F-BNNTs within a wide range of F atom concentrations. When the fluorination level is changed from 1.0% (1/96) to 8.3% (2/24) by simply decreasing or increasing F atoms within the F chain, the magnetic moment per chemisorption changes largely, in the range of 0.37−1.0 μ_B (see the Supporting Information for detailed results). On the other hand, the fluorination level can also be increased by placing an additional F chain at the diametrically opposite side of the nanotube. Taking the (10,0) F-BNNT shown in Figure 1c as an example, total energy calculations show that the FM state is 42 meV per unit cell more stable than the nonmagnetic one. In this F-BNNT, the coupling between the spins from two F chains is also ferromagnetic, which is 4 meV per unit cell more favorable than the AFM coupling. This forms a striking contrast to the zigzag graphene nanoribbons where the spin

(43) Mahadevan, P.; Zunger, A.; Sarma, D. D. *Phys. Rev. Lett.* **2004**, *93*, 177201.
(44) R. J. Jr.; Byers, S. J. M.; Osofsky, M. S.; Nadgorny, B. *Science* **1998**, *282*, 85–88.
(45) Yang, C. K.; Zhao, J.; Lu, J. P. *Phys. Rev. Lett.* **2003**, *90*, 257203.
(46) The extra charges are induced into the systems by adjusting the charge neutrality level, with a uniform jellium countercharge.

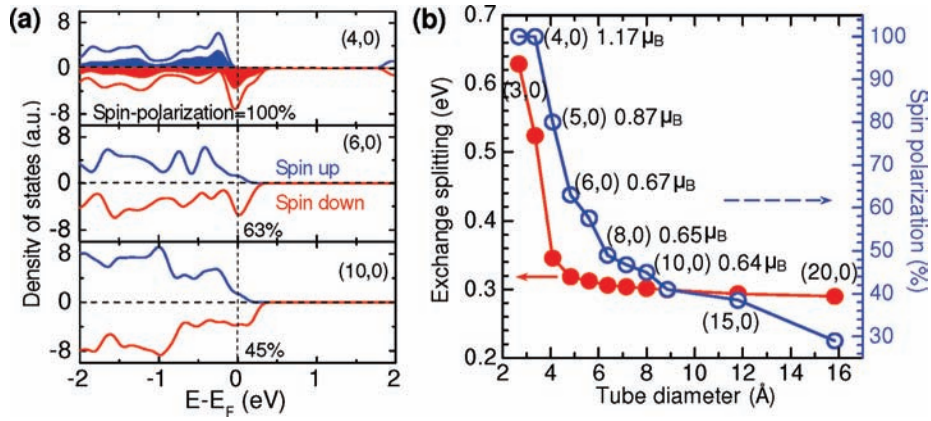

Figure 3. Diameter dependence of the spin polarization and magnetic moment in F-BNNTs. (a) Spin-resolved density of states of the (4,0), (6,0), and (10,0) F-BNNTs (bottom, minority spin; top, majority spin). Color shaded areas represent the corresponding nitrogen 2p states of the (4,0) F-BNNT. The Fermi level is set to zero. (b) Exchange splitting of band I (see Figure 2a) and spin polarization as a function of diameter of the (*n*,0) F-BNNT.

coupling between two ribbon edges is AFM.[15−17] For intrachain spin interaction, the FM ordering is 30 meV per unit cell more stable than the AFM ordering. The magnetic moment is calculated to be 0.32 μ_B/Å, which is nearly 1 order higher than that of the CNTs with topological line defects reported in ref 17. In a word, the spin ordering in the F-BNNTs is robust within a wide range of fluorination levels.

Size effect is always important in nanosystems. So we investigate the size dependence of the spin ordering in F-BNNTs by varying the tube from (4,0) to (11,0). It is found that the magnetic moment increases monotonically with decreasing tube size, from 0.63 μ_B in the (11,0) F-BNNT to 1.17 μ_B in the (4,0) F-BNNT, with the corresponding spin polarization increasing from 38% to 100% as shown in Figure 3b. More importantly, the interaction between the defect-induced moments keeps FM coupling independent of tube size. The strongly size-dependent FM spin ordering can be mapped to adsorption energy[47] of the F atom, which is reduced from 3.9 eV in the (4,0) F-BNNT to 2.6 eV in the (11,0) F-BNNT. This is also well reflected by the change in the calculated F−B bond length, from 1.36 Å in the (4,0) to 1.4 Å in the (11,0) F-BNNT. The size-dependent spin polarization roots in the exchange splitting of the defect band I, which decreases with increasing tube diameter as shown by Figure 3b. We explain this variation from two aspects. First, with increasing tube diameter, the defect states need to delocalize to lower the total energy of the system due to weaker binding between the F and the BNNT, which is demonstrated clearly by the change of defect band dispersion with tube diameter. The dispersion of band I increases from 0.17 eV for the (6,0) F-BNNT to 0.30 eV for the (11,0) F-BNNT. This delocalization of defect states leads to reduction of the exchange splitting. Second, the hole population in the BNNT decreases with increasing tube diameter as well. This leads to a slight increase in occupancy of the defect bands, giving rise to the reduction of exchange splitting. Simple electron counting indeed shows that holes in the (11,0) F-BNNT are 0.07|e| less than those in the (6,0) F-BNNT. Therefore, the combined effects of delocalization of the defect states and depopulation of holes in the system are responsible for the decrease of spin polarization with increasing tube diameter.

Half-metal can make the electrons with one spin orientation transmitted and the electrons with the other insulated, which is rarely found in 1D sp materials.[48,49] The 100% spin polarization in the (4,0) F-BNNT with diameter of 3.3 Å indicates that the half-metal is realized. Furthermore, careful calculations show that the (4,0) is a critical size for the half-metal, below which all F-BNNTs become half-metallic as well. This is meaningful because our recent calculations show that even the (3,0) BNNT can be stable well over room temperature.[50] The spin-polarized DOS for the (4,0) F-BNNT is shown in Figure 3a, where substantial electronic states are found around the Fermi level for minority spin, while no state is observed for majority spin. So electric transport through the (4,0) F-BNNT is carried out solely by carriers with minority spin state, mainly from the nitrogen 2p states.

Motivated by this radial dependence, we guess that the relatively weak FM ordering in large F-BNNTs can be enhanced by increasing local tube curvature. This would be very practical as large-diameter F-BNNTs are easier to synthesize. Moreover, because single-walled BNNTs have been shown to exhibit significant reversible radial deformability, radial compression to the F-BNNTs may lead to tunable spin ordering. We squash the BNNT along the *y* direction as shown in the inset of Figure 4a, and the radial strain is defined as $\varepsilon_{yy} = (D - D_y)/D$, where D is the diameter of the undeformed BNNT and D_y is the minor axes of the deformed elliptical BNNT. For different radial strain ε_{yy}, the structure is fully relaxed except for the atoms at the squashed sites. We only discuss the adsorption of F atom on the high curvature site as it results in the highest adsorption energy. Figure 4a shows the variation in spin polarization of F-BNNTs with ε_{yy}. It is shown that the spin polarization of the squashed (20,0) F-BNNT with $\varepsilon_{yy} = 0.73$ reaches up to 80%, about 176% enhanced over the undeformed level. The spin polarizations of the (15,0) and (10,0) F-BNNTs also show 87% and 46% enhancement over their undeformed levels at $\varepsilon_{yy} =$ 0.64 and 0.54, respectively. However, there is a critical radial strain above which the spin polarization rapidly decreases with further increasing strain, different from the change in adsorption energy per F atom that monotonically increases with ε_{yy}. The rapid reduction of spin polarization under high radial strain may find applications in nanodevices, such as a mechanical switch for spin-polarized transport.

(47) Adsorption energy is calculated by subtracting the total energy of the F-BNNT from the total energies of a pristine BNNT and an isolated F atom in the triplet state, with the same calculating parameters.

(48) Son, Y.; Cohen, M. L.; Louie, S. G. *Nature* **2007**, *444*, 347–349.
(49) Kan, E.; Li, Z.; Yang, J.; Hou, J. G. *J. Am. Chem. Soc.* **2008**, *130*, 4224–4225.
(50) Zhang, Z. H.; Guo, W. L.; Dai, Y. T. *Appl. Phys. Lett.* **2008**, *93*, 223108.

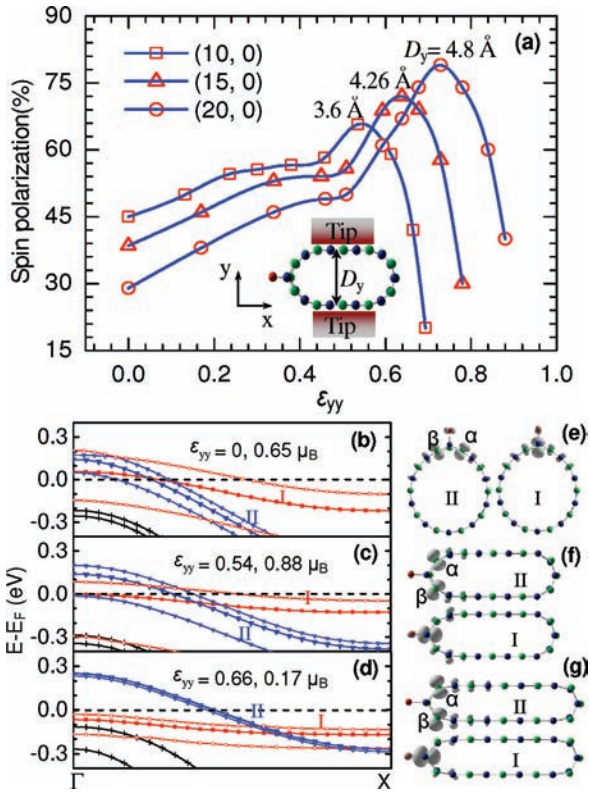

Figure 4. Tunable spin polarization in F-BNNTs by radial deformation. (a) Spin polarization as a function of radial strain ε_{yy}. Insert illustrates the (10,0) F-BNNT compressed along the y direction. (b−d) Band structures of the (10,0) F-BNNT with ε_{yy}= 0 (b), 0.54 (c), and 0.66 (d). The lines with little hollow symbols show the spin splitting for bands I and II. Magnetic moments of the system under the corresponding strains are also displayed. (e−g) Iso-surface (0.15 e/Å^3) plots of the corresponding charge density for bands I and II at ε_{yy} = 0 (e), 0.54 (f), and 0.66 (g).

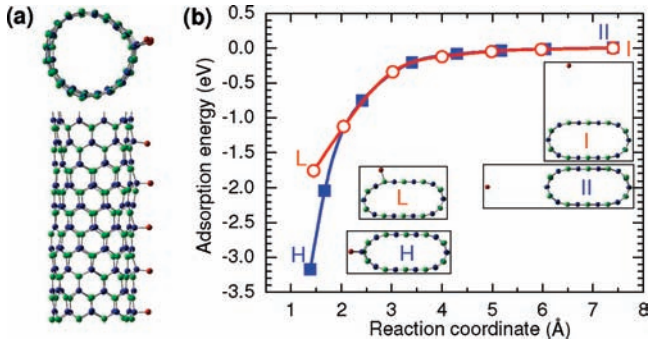

Figure 5. The stability and reactivity of 1D fluorine chain adsorbed on the (10,0) BNNT. (a) Axial and lateral views of the relaxed atomic configurations of the (10,0) F-BNNT after 3 ps ab initio molecular dynamics simulations at 800 K. (b) Calculated minimum energy path between the physisorption and chemisorption states for a fluorine atom on the high curvature and low curvature sites of a squashed (10,0) BNNT.

Explanation of this interesting change of the spin polarization with ε_{yy} is sought in the band structures. Figure 4b−d shows the band structures around the Fermi level for the (10,0) F-BNNT with ε_{yy} = 0, 0.54, and 0.66, respectively. We focus on bands I and II as they determine the magnetic behavior of the system. It is found that the localization of bands I and II is strengthened continuously with increasing ε_{yy}, in line with the change of F atom adsorption energy. However, when the spin degrees of freedom are switched on, the discussion should be divided into two steps. First, when ε_{yy} is increased from 0 to 0.54, the exchange splitting of both bands is remarkably enhanced as shown in Figure 4b,c, which directly leads to the enhancement of the spin polarization, whereas in the second step, by further increasing ε_{yy} to 0.66, the exchange splitting is largely weakened, especially for band II, although the holes are almost distributed within it (Figure 4d). To better understand this change, we plot the charge densities for bands I and II at the corresponding ε_{yy} in Figure 4e−g. It is shown that the charge density of band II is mainly localized on the two opposite N atoms bonding to the adsorption site as denoted by α and β, respectively. Evidently, squashing the nanotube can enhance the $\pi-\pi$ interaction between the α and β atoms, which not only raises band II to a higher level but enables the formation of weak covalent bonds. At high radial strains, the nitrogen 2p states are largely involved in the bond formation and are no longer able to cause the exchange splitting, making the magnetism quenched rapidly. It thus is concluded that the change of spin polarization with radial strain results from the interesting interplay between the localization of the defect states and the $\pi-\pi$ interaction.

We also note that the magnetic modulation is more remarkable and more facile in larger F-BNNT. Figure 4a shows that the highest spin polarization available in the modulation process increases with increasing tube diameter. The peak value of spin polarization for the (20,0) F-BNNT is 10% higher than that for the (15,0) F-BNNT and 21% than that for the (10,0) F-BNNT. This is because a larger F-BNNT can bear a higher radial strain before the $\pi-\pi$ interaction between the squashed faces reacts. From the strain energy under radial deformation, we can roughly estimate the pressures involved in the critical radial strains. Assuming that forces act on the flat areas of tube along the radial direction, the pressure is estimated to be about 1.2 GPa for the (15,0) F-BNNT at ε_{yy} = 0.64 (D_y = 4.26 Å), much lower than that of 7.8 GPa for the (10,0) F-BNNT at ε_{yy} = 0.54 (D_y = 3.6 Å). It is important that the critical radial strains are still in the elastic range. The present strategy is expected to be applicable to other classes of nanotubes, such as GaN nanotubes, thus highlighting a new direction for piezomagnetic devices.

To clarify the stability and reactivity of the proposed F-BNNT, we performed energetics and dynamics calculations. First, we calculated the formation energies of a fluorinated and a clean (10,0) BNNT (see ref 51 for details). The formation energy is calculated to be 46 meV/atom for the (10,0) F-BNNT, even distinctly lower than that of 85 meV/atom for a clean (10,0) BNNT. The striking reduction of formation energy induced by fluorination is due to the larger binding energy of F−B bond (4.15 eV) than that of F−F bond (2.08 eV). Therefore, the F-BNNT is energetically stable. Indeed, after a 3 ps ab initio MD simulation for the (10,0) F-BNNT with a large supercell including 205 atoms, we do not observe any signs of F desorption or F chain disruption at temperature up to 800 K (Figure 5a). Recent experiment also observed that termination with F atoms can largely reduce the (001) surface energy of anatase TiO_2 single crystals.[52] Finally, we proposed a mechan-

(51) For a F-BNNT, the formation energy per atom is calculated as $\delta G = E_{coh}-(1-x)(\mu_B+\mu_N)/2-x\mu_F$, where E_{coh} is the cohesive energy per atom of the F_xBN nanotube, x is the molar fraction of F atom in the nanotube, and μ_i (i = B, N, F) is the corresponding chemical potential at a given state. We choose $\mu_B+\mu_N$ as the cohesive energy per BN pair of a h-BN sheet, and μ_F as the binding energy per atom of a F_2 molecule. Positive δG means that the system is metastable with respect to a flat BN sheet.

(52) Yang, H. G.; Sun, C. H.; Qiao, S. Z.; Zou, J. *Nature* **2008**, *453*, 638–641.

ical method for biasing the F chemisorption along the tube axis by radially compressing the BNNTs. Figure 5b shows the MEPs for adsorption of F atoms onto the high and low curvature sites of a deformed (10,0) BNNT with $\varepsilon_{yy} = 0.5$. It is found that when F atoms start to bind with the tube wall, the adsorption at low curvature site is energetically less favorable than that at high curvature site. The final adsorption configuration at high curvature site (B) can be 1.4 eV more stable than the configuration at the low curvature site (A). Therefore, configuration A may become unstable with rising temperature, and the adsorbed F atoms should diffuse to the high curvature regions. To confirm this prediction, we performed annealing MD simulations of configuration A with 205 atoms per supercell. After annealing for 5000 MD steps (25 ps), slowly decreasing the temperature from 1300 to 50 K, we find that most of the F atoms in this configuration transfer to the high curvature regions of the tube. As a result, the F-BNNT of Figure 1c can be obtained at the appropriate fluorine concentration. Increasing the radial strain can further enhance the biasing effect of fluorination. These results also have implications for many bistable devices utilizing deformed nanotubes where the curvature change is expected to significantly alter the chemical behavior important to their applications.

Summary

In summary, systematic first-principles calculations reveal that BNNTs with topological fluorine adsorption can exhibit long-ranged ferromagnetic spin ordering along the tube as well as strong spin polarization around the Fermi level. The F-BNNTs thus can serve as ferromagnetic nanowires consisting solely of sp-elements. The spin polarization and magnetic moment increase rapidly with decreasing tube diameter, even giving rise to half-metal in the (4,0) or smaller F-BNNTs. By radially compressing the F-BNNT, the magnetism can also be dramatically enhanced up to a critical radial strain in elastic range, with more remarkable enhancement in larger F-BNNT, and then be rapidly quenched with further increasing radial strain. Magnetism enhancing or quenching can also be realized by injection of holes or electrons into the system. Further experimental studies are expected to confirm the attractive predictions.

Acknowledgment. This work was supported by the 973 Program (2007CB936204), National NSF (10732040), the Jiangsu Province NSF (BK2008042), the MOE (705021, IRT0534) of China, and Jiangsu Province Scientific Research Innovation Project for Graduate Student (CX07B_064z). We thank Professor Changfeng Chen (UNLV) and Professor Xiaocheng Zeng (UNL) for helpful discussions.

Supporting Information Available: Effect of F atom concentrations on the observed magnetism. This material is available free of charge via the Internet at http://pubs.acs.org.

JA901586K